Neuron, Volume *111*

Supplemental information

Customization of the translational complex regulates mRNA-specific translation to control CNS regeneration

Julia Schaeffer, Noemie Vilallongue, Charlotte Decourt, Beatrice Blot, Nacera El Bakdouri, Elise Plissonnier, Blandine Excoffier, Antoine Paccard, Jean-Jacques Diaz, Sandrine Humbert, Frederic Catez, Frederic Saudou, Homaira Nawabi, and Stephane Belin

Supplementary Figure 1

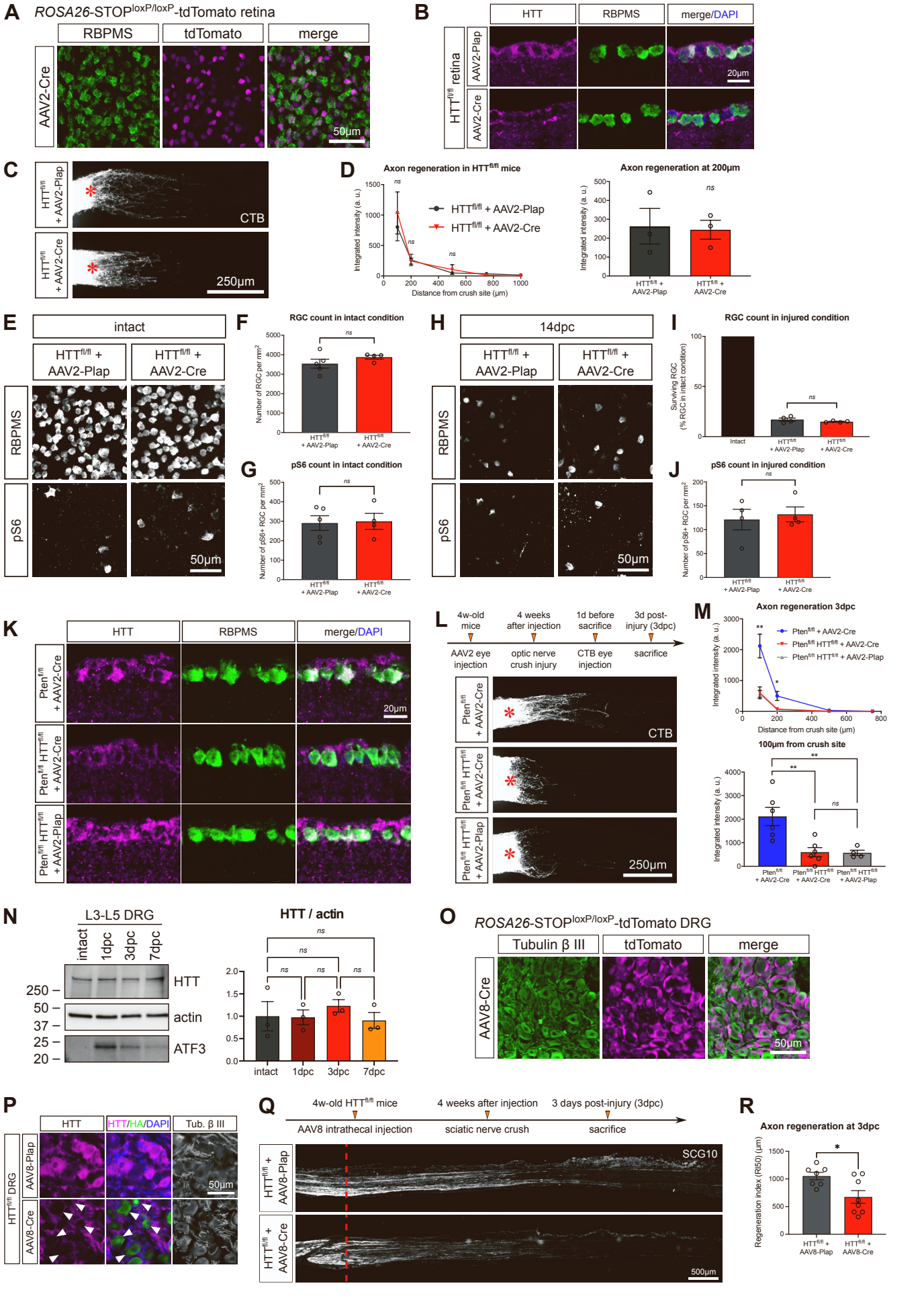

Figure S1: Axon regeneration and RGC survival are not modified by HTT deletion in wild-type condition, related to Figure 1.

(A) Representative confocal image of whole-mount retina of *ROSA26*-STOP$^{loxP/loxP}$-tdTomato mouse, showing tdTomato expression in RBPMS^{+} RGC.

(B) Representative confocal images showing HTT protein expression in HTT$^{fl/fl}$+AAV2-Plap and HTT$^{fl/fl}$+AAV2-Cre RBPMS^{+} RGC.

(C) Whole optic nerve confocal images showing CTB^{+} regenerating axons in HTT$^{fl/fl}$+AAV2-Plap and HTT$^{fl/fl}$+AAV2-Cre conditions at 14dpc. The injury site is indicated by a red star.

(D) Quantification of integrated fluorescence intensity along the optic nerve. Data are represented as mean +/- s.e.m. Unpaired t-test, ns: not significant.

(E) Whole-mount retina confocal images showing RBPMS^{+} RGC and pS6^{+} RGC in HTT$^{fl/fl}$+AAV2-Plap and HTT$^{fl/fl}$+AAV2-Cre in intact condition.

(F) Quantification of RBPMS^{+} RGC per mm^{2} retina in intact condition. Data are represented as mean +/- s.e.m. Unpaired t-test, ns: not significant.

(G) Quantification of pS6^{+} RGC per mm^{2} retina in intact condition. Data are represented as mean +/- s.e.m. Unpaired t-test, ns: not significant.

(H) Whole-mount retina confocal images showing RBPMS^{+} and pS6^{+} RGC in HTT$^{fl/fl}$+AAV2-Plap and HTT$^{fl/fl}$+AAV2-Cre conditions at 14dpc.

(I) Quantification of RBPMS^{+} RGC as a percentage of intact RBPMS^{+} RGC at 14dpc. Data are represented as mean +/- s.e.m. Unpaired t-test, ns: not significant.

(J) Quantification of pS6^{+} RGC per mm^{2} retina at 14dpc. Data are represented as mean +/- s.e.m. Unpaired t-test, ns: not significant.

(K) Representative confocal images showing HTT protein expression in Pten$^{fl/fl}$+AAV2-Cre, Pten$^{fl/fl}$HTT$^{fl/fl}$+AAV2-Cre and Pten$^{fl/fl}$HTT$^{fl/fl}$+AAV2-Plap intact RBPMS^{+} RGC.

(L) Schematic timeline and representative results of optic nerve crush injury experiment. Whole optic nerve confocal images showing CTB^{+} regenerating axons in Pten$^{fl/fl}$+AAV2-Cre, Pten$^{fl/fl}$HTT$^{fl/fl}$+AAV2-Cre and Pten$^{fl/fl}$HTT$^{fl/fl}$+AAV2-Plap conditions at 3dpc. The injury site is indicated by a red star.

(M) Quantification of integrated fluorescence intensity along the optic nerve. Data are represented as mean +/- s.e.m. One-way ANOVA with Bonferroni multiple comparisons test, *p-value<0.05, **p-value<0.01, ***p-value<0.001, ns: not significant. The top graph gives the multiple comparisons test between Pten$^{fl/fl}$+AAV2-Cre and Pten$^{fl/fl}$HTT$^{fl/fl}$+AAV2-Cre conditions.

(N) Immunoblot and quantification of L3 to L5 DRG lysate showing HTT, actin and ATF3 protein expression in intact condition and at different timepoints after sciatic nerve injury. Data are represented as mean +/- s.e.m. One-way ANOVA with Bonferroni multiple comparisons test, ns: not significant.

(O) Representative epifluorescence image of DRG section from *ROSA26*-STOP$^{loxP/loxP}$-tdTomato mouse, injected intrathecally with AAV8-Cre, showing tdTomato expression in Tubulin β III^{+} DRG neurons.

(P) Representative epifluorescence images showing HTT protein expression in $HTT^{fl/fl}$+AAV8-Plap and $HTT^{fl/fl}$+AAV8-Cre DRG. Neurons infected with AAV8-Cre are HA^{+}.
(Q) Epifluorescence images showing regeneration of DRG axons in the sciatic nerve in $HTT^{fl/fl}$+AAV8-Plap and $HTT^{fl/fl}$+AAV8-Cre at 3dpc. Regenerating axons are labeled with anti-SCG10 antibody. The injury site is indicated by a red dashed line.
(R) Quantification of the regeneration index calculated as the distance to the injury site for which axon regeneration is 50% of the intact region. Data are represented as mean +/- s.e.m. Unpaired t-test, *p-value<0.05.

Supplementary Figure 2

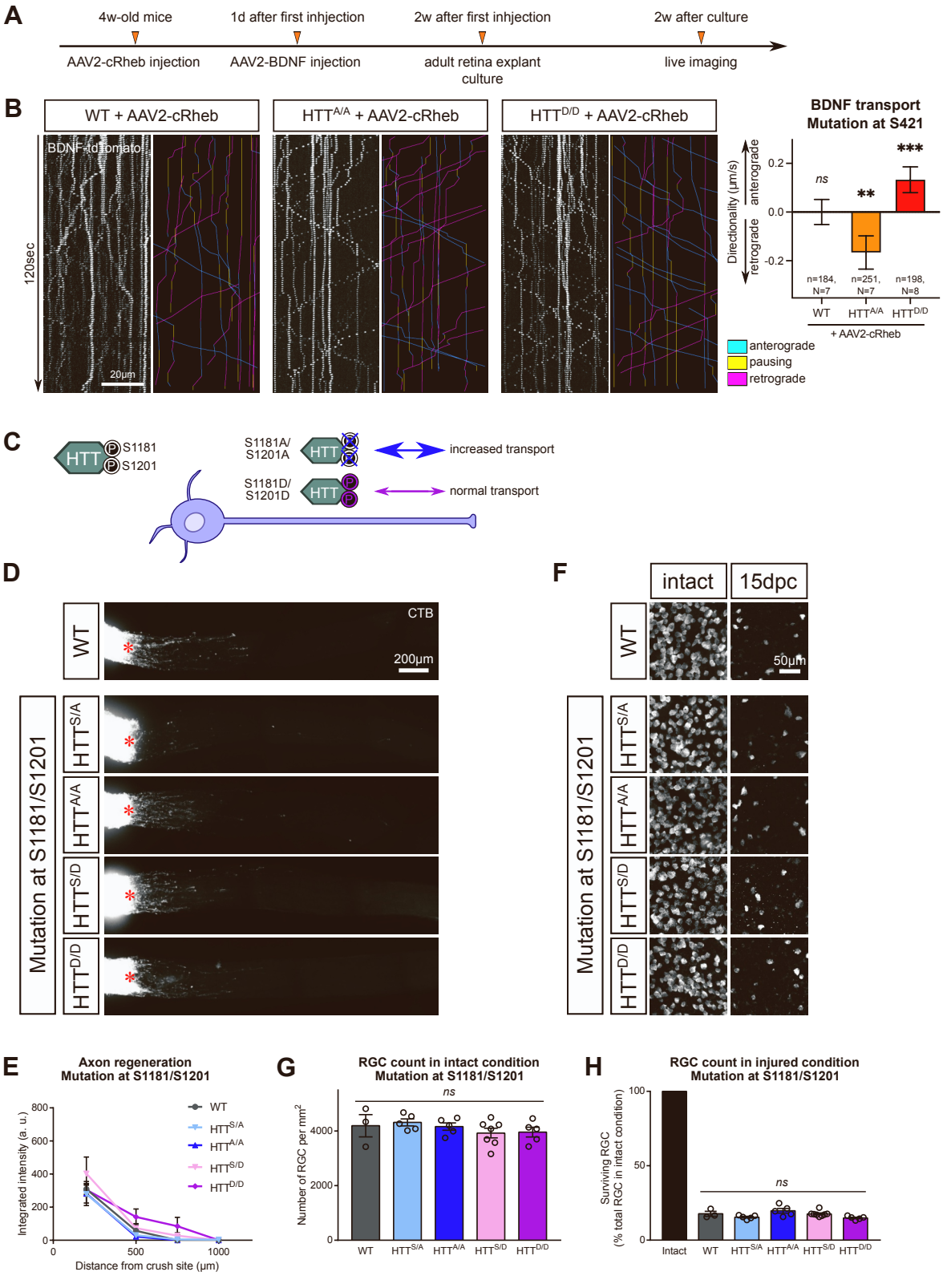

Figure S2: Axon regeneration and RGC survival are not modified by S1181/S1201 phospho-mutations responsible for HTT-mediated control of BDNF transport, related to Figure 2.

(A) Schematic timeline of adult retina explant culture set-up.

(B) Representative kymographs of BDNF vesicle transport in WT axons or in axons from HTT phospho-mutant mice (mutation at S421, A/A or D/D). Quantification of directionality. Data are represented as mean +/- s.e.m., with n the number of vesicles and N the number of independent axons. Wilcoxon signed-rank test with comparison of median to theoretical value of 0, **p-value<0.01, ***p-value<0.001.

(C) Schematic representation of transgenic mouse lines carrying S1181/S1201 phospho-point mutations [S1].

(D) Whole optic nerve confocal images showing CTB^+ regenerating axons in phospho-mutant mouse lines at 15dpc. The injury site is indicated by a red star.

(E) Quantification of integrated fluorescence intensity along the optic nerve.

(F) Whole-mount retina confocal images showing $RBPMS^+$ RGC in phospho-mutant mouse lines in intact and 15dpc conditions.

(G) Quantification of $RBPMS^+$ RGC per mm^2 retina in intact condition. Data are represented as mean +/- s.e.m. One-way ANOVA with Bonferroni multiple comparisons test, ns: not significant.

(H) Quantification of $RBPMS^+$ RGC as a percentage of intact $RBPMS^+$ RGC. Data are represented as mean +/- s.e.m. One-way ANOVA with Bonferroni multiple comparisons test, ns: not significant.

Supplementary Figure 3

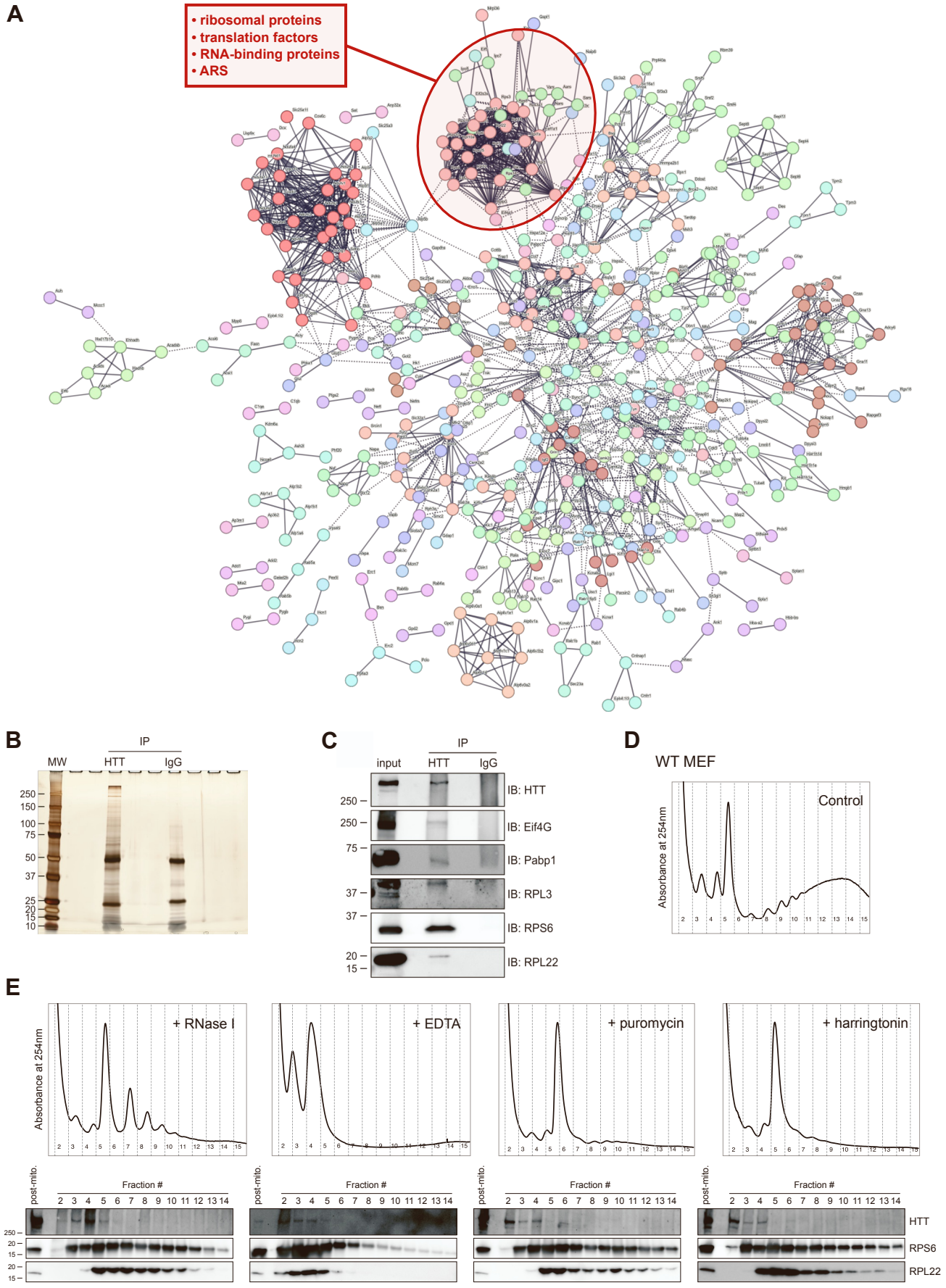

Figure S3: HTT binding partners include components of the translation machinery, related to Figure 3.

(A) STRING interactome of 747 HTT binding partners identified by affinity purification and mass spectrometry analysis by Shirasaki and colleagues [S2]. Network edges represent confidence with minimum interaction score of 0.9 (highest confidence). Disconnected nodes in the network are hidden from the representation. ARS: aminoacyl tRNA synthetases. A high-resolution version of this graph is available in **Supplemental Table 1**.

(B) Silver staining of anti-HTT immunoprecipitated proteins versus IgG control from WT MEF lysate.

(C) Immunoblot of proteins immunoprecipitated with anti-HTT from WT MEF lysate.

(D) Representative polysome profile of WT MEF on a 15-50% sucrose gradient.

(E) Representative polysome profile of WT MEF on a 15-50% sucrose gradient, with previous treatments of cells (puromycin, harringtonin) or lysates (EDTA, RNase I). Corresponding immunoblots showing HTT distribution in the different fractions.

Supplementary Figure 4

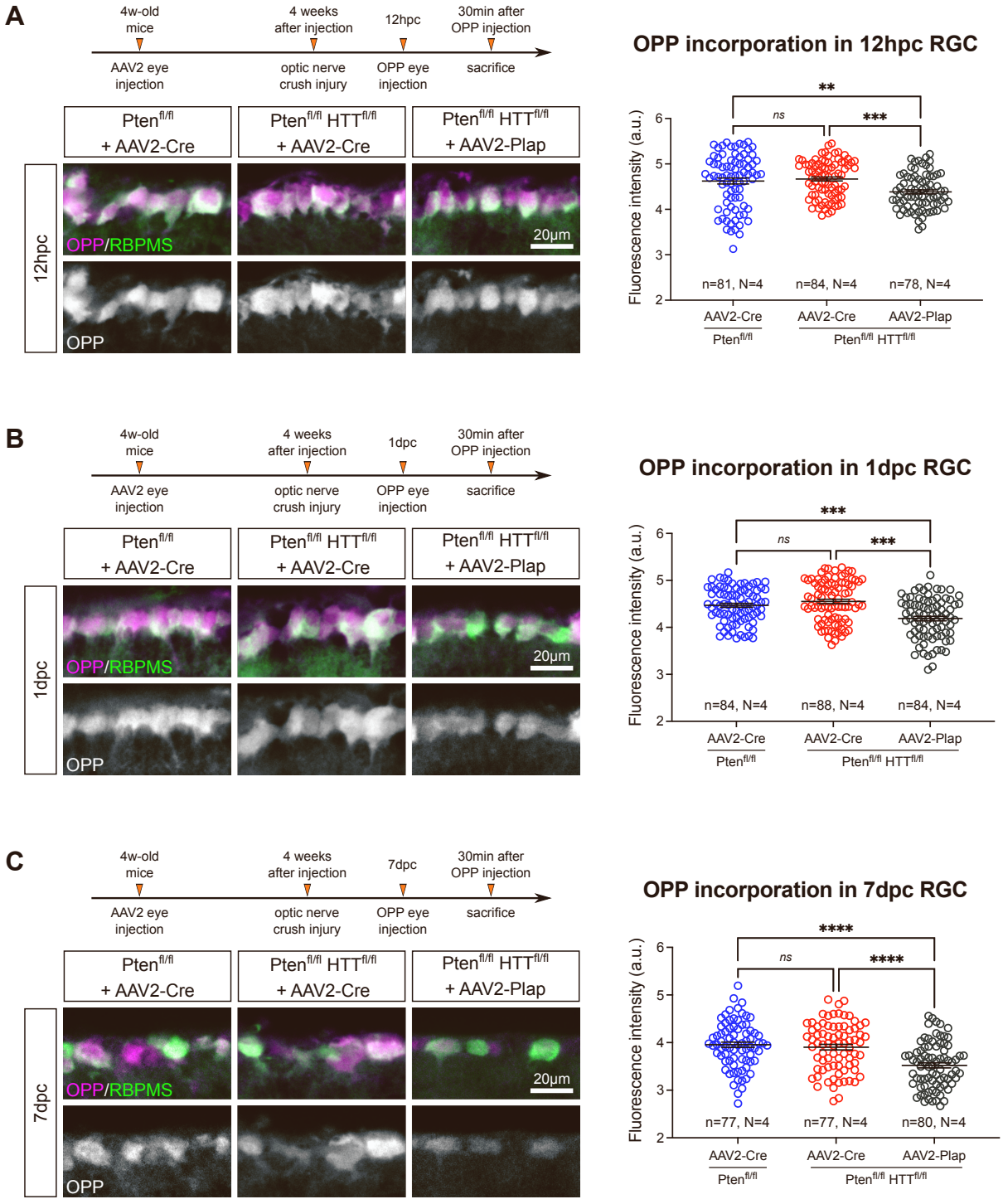

Figure S4: HTT deletion does not modify global translation in injured Pten-deleted RGC, related to Figure 4.

(A) Representative images and quantification of OPP incorporation in $Pten^{fl/fl}$+AAV2-Cre, $Pten^{fl/fl}HTT^{fl/fl}$+AAV2-Cre and $Pten^{fl/fl}HTT^{fl/fl}$+AAV2-Plap RGC at 12hpc.

(B) Representative images and quantification of OPP incorporation in $Pten^{fl/fl}$+AAV2-Cre, $Pten^{fl/fl}HTT^{fl/fl}$+AAV2-Cre and $Pten^{fl/fl}HTT^{fl/fl}$+AAV2-Plap RGC at 1dpc.

(C) Representative images and quantification of OPP incorporation in $Pten^{fl/fl}$+AAV2-Cre, $Pten^{fl/fl}HTT^{fl/fl}$+AAV2-Cre and $Pten^{fl/fl}HTT^{fl/fl}$+AAV2-Plap RGC at 7dpc.

Data are represented as mean +/- s.e.m. One-way ANOVA with Bonferroni multiple comparisons test, **p-value<0.01, ***p-value<0.001, ns: not significant.

Supplementary Figure 5

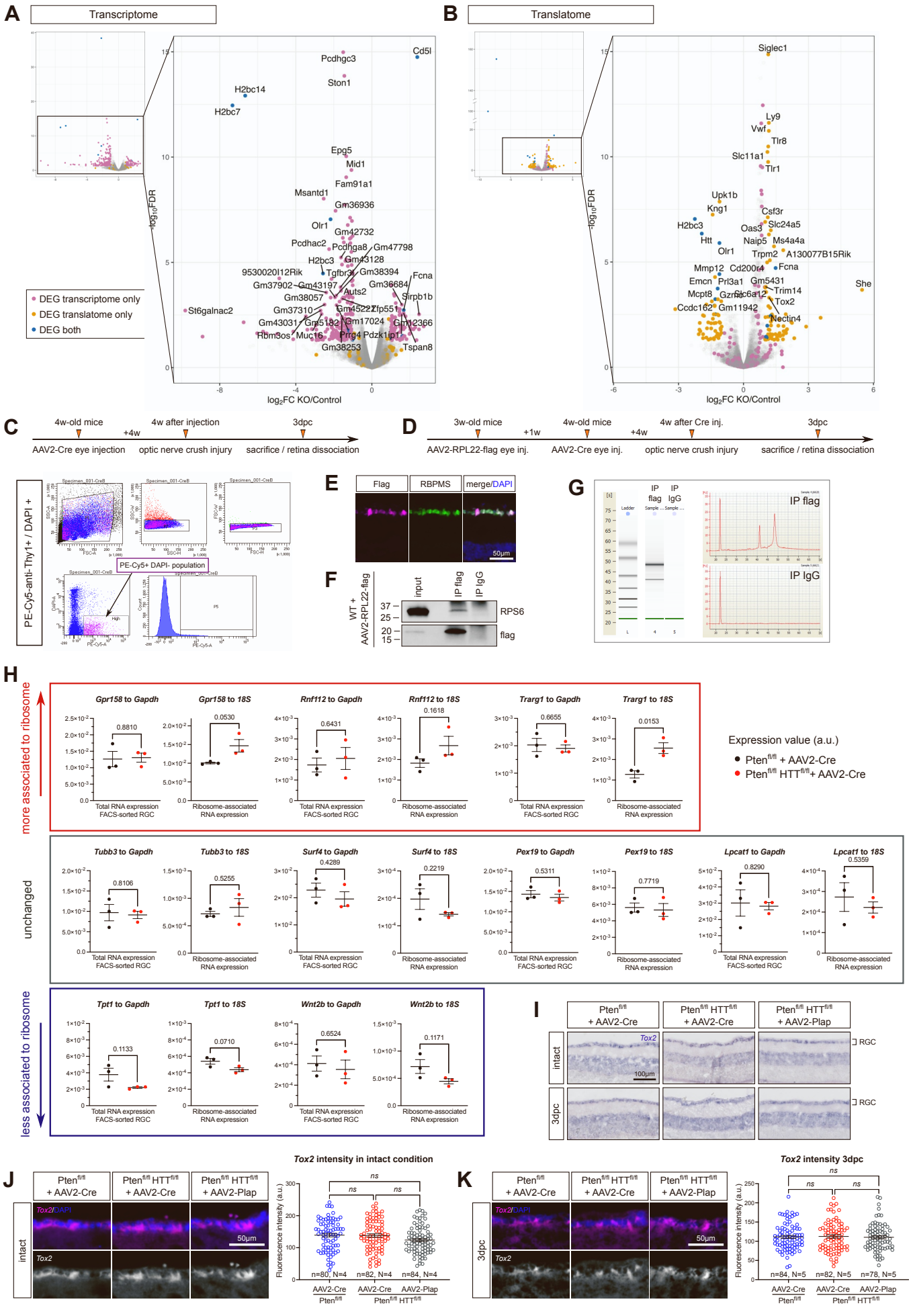

Figure S5: Comparison of transcriptome and translatome in control and HTT KO MEF shows mRNA-specific regulation of translation, related to Figure 5.

(A) Volcano plot showing $-\log_{10}$(FDR-adjusted p-value) as a function of the $\log_2$(fold-change HTT-KO versus control) in total RNA samples. Blue hits: FDR-corrected p-value<0.05 and $|\log_2(\text{fold-change})|>1$ in both datasets. Pink hits: FDR-corrected p-value<0.05 and $|\log_2(\text{fold-change})|>1$ in transcriptome only. Orange hits: FDR-corrected p-value<0.05 and $|\log_2(\text{fold-change})|>1$ in translatome only.

(B) Volcano plot showing $-\log_{10}$(FDR-adjusted p-value) as a function of the $\log_2$(fold-change HTT-KO versus control) in translated RNA samples.

(C) Schematic timeline of RGC cell sorting from $Pten^{fl/fl}$+AAV2-Cre versus $Pten^{fl/fl}HTT^{fl/fl}$+AAV2-Cre retinas. Representative FACS plots illustrating the steps of RGC isolation. Dissociated retinal cells are gated based on size and surface characteristics (forward scatter, FSC; side scatter, SSC). PE-Cy5-Thy1-positive DAPI-negative population was selected. Double negative staining of retinal cells was used as a control to set up the threshold for PE-Cy5 and DAPI.

(D) Schematic timeline of ribosome immunoprecipitation from RGC of $Pten^{fl/fl}$+AAV2-Cre versus $Pten^{fl/fl}HTT^{fl/fl}$+AAV2-Cre retinas.

(E) Representative immunofluorescence image showing flag expression in $RBPMS^{+}$ RGC of AAV2-RPL22-flag-injected mice.

(F) Representative immunoblot of anti-flag- and control IgG-immunoprecipitated proteins from retina lysate of WT mice injected with RPL22-flag.

(G) Representative Bioanalyzer profiles of translated RNA isolated after anti-flag and control IgG immunoprecipitation.

(H) RT-qPCR analysis of selected mRNA levels in total RNA samples and in ribosome-associated RNA samples. For each tested mRNA, the expression level is normalized to *Gapdh* level for total RNA isolated from FACS-sorted RGC; and *18S* level in ribosome-associated RNA fraction. Levels are compared between $Pten^{fl/fl}$+AAV2-Cre and $Pten^{fl/fl}HTT^{fl/fl}$+AAV2-Cre conditions at 3dpc. Data are represented as mean +/- s.e.m. The p-value corresponding to unpaired t-test is displayed on each graph.

(I) In situ hybridization showing *Tox2* mRNA expression in $Pten^{fl/fl}$+AAV2-Cre, $Pten^{fl/fl}HTT^{fl/fl}$+AAV2-Cre and $Pten^{fl/fl}HTT^{fl/fl}$+AAV2-Plap in intact and 3dpc conditions.

(J) Fluorescent in situ hybridization and quantification of *Tox2* mRNA expression in $Pten^{fl/fl}$+AAV2-Cre, $Pten^{fl/fl}HTT^{fl/fl}$+AAV2-Cre and $Pten^{fl/fl}HTT^{fl/fl}$+AAV2-Plap intact RGC. Data are represented as mean +/- s.e.m. One-way ANOVA with Bonferroni multiple comparisons test, ns: not significant.

(K) Fluorescent in situ hybridization and quantification of *Tox2* mRNA expression in $Pten^{fl/fl}$+AAV2-Cre, $Pten^{fl/fl}HTT^{fl/fl}$+AAV2-Cre and $Pten^{fl/fl}HTT^{fl/fl}$+AAV2-Plap at 3dpc. Data are represented as mean +/- s.e.m. One-way ANOVA with Bonferroni multiple comparisons test, ns: not significant.

Supplementary Figure 6

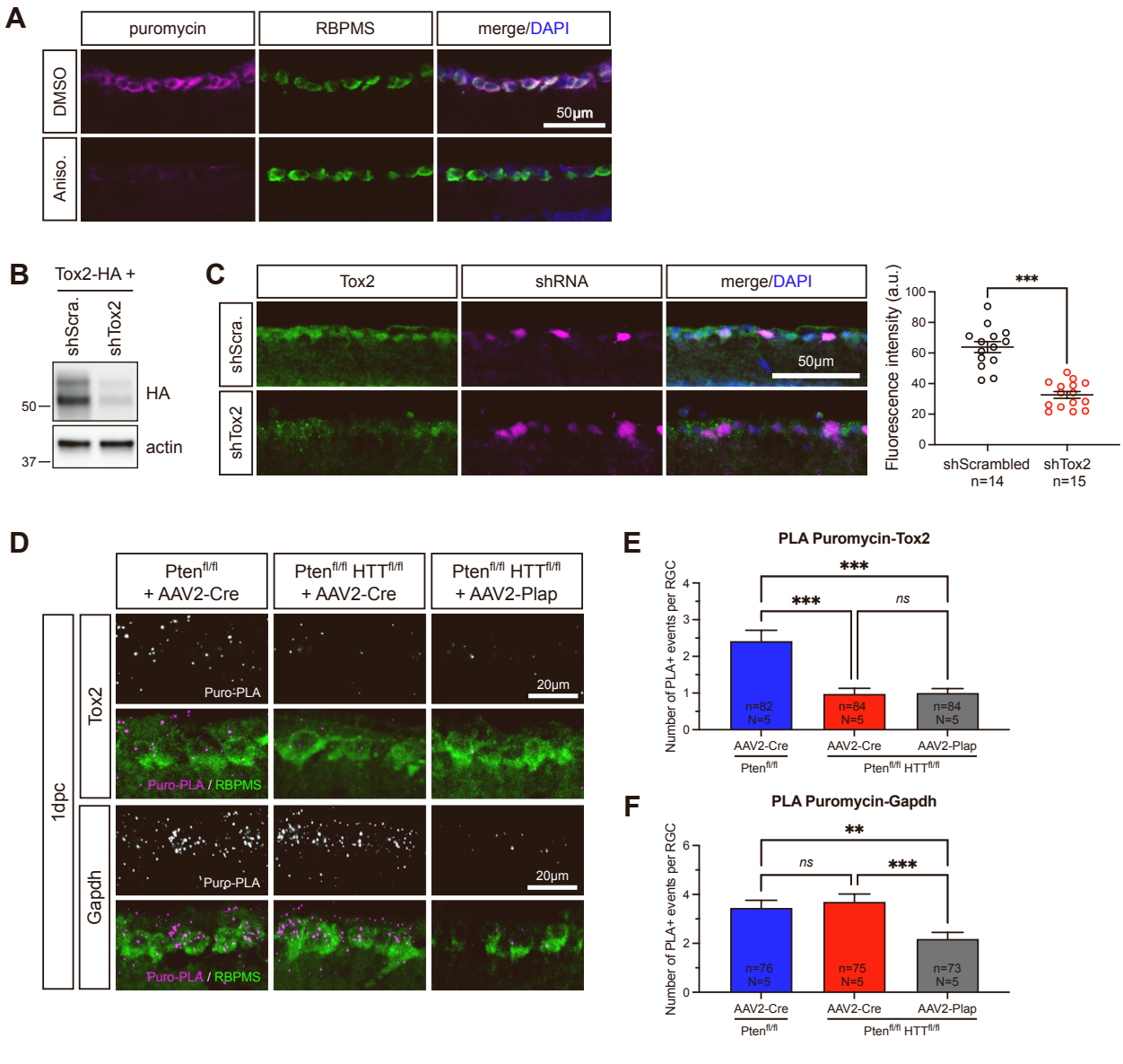

Figure S6: Tox2 is translationally-regulated by HTT in vivo after injury, related to Figure 6.

(A) Representative immunofluorescence images using anti-puromycin antibody in WT RGC with DMSO or Anisomycin injection, and with OPP injection 30min before sacrifice. Data are represented as mean +/- s.e.m. Unpaired t- test, **p-value<0.01, ns: not significant.

(B) Validation of shRNA against Tox2 (shTox2) by immunoblot using overexpression of Tox2-HA in mouse N2A cells.

(C) Validation of shRNA against Tox2 (shTox2) by immunofluorescence with anti-Tox2 antibody in mouse RGC. Quantification of immunofluorescence intensity in individual RGC expressing shScrambled or shTox2 ($mCherry^{+}$ cells). Data are represented as mean +/- s.e.m. Unpaired t-test, ***p-value<0.001.

(D) PLA staining confocal images for puromycin-Tox2 or puromycin-Gapdh in $Pten^{fl/fl}$+AAV2-Cre, $Pten^{fl/fl}HTT^{fl/fl}$+AAV2-Cre and $Pten^{fl/fl}HTT^{fl/fl}$+AAV2-Plap RGC at 1dpc.

(E) Quantification of puromycin-Tox2 PLA-positive events in $Pten^{fl/fl}$+AAV2-Cre, $Pten^{fl/fl}HTT^{fl/fl}$+AAV2-Cre and $Pten^{fl/fl}HTT^{fl/fl}$+AAV2-Plap RGC at 1dpc. Data are represented as mean +/- s.e.m. Kruskal-Wallis with Dunn's multiple comparisons test, ***p-value<0.001, ns: not significant.

(F) Quantification of puromycin-Gapdh PLA-positive events in $Pten^{fl/fl}$+AAV2-Cre, $Pten^{fl/fl}HTT^{fl/fl}$+AAV2-Cre and $Pten^{fl/fl}HTT^{fl/fl}$+AAV2-Plap RGC at 1dpc. Data are represented as mean +/- s.e.m. Kruskal-Wallis with Dunn's multiple comparisons test, **p-value<0.01, ***p-value<0.001, ns: not significant.

Supplementary Figure 7

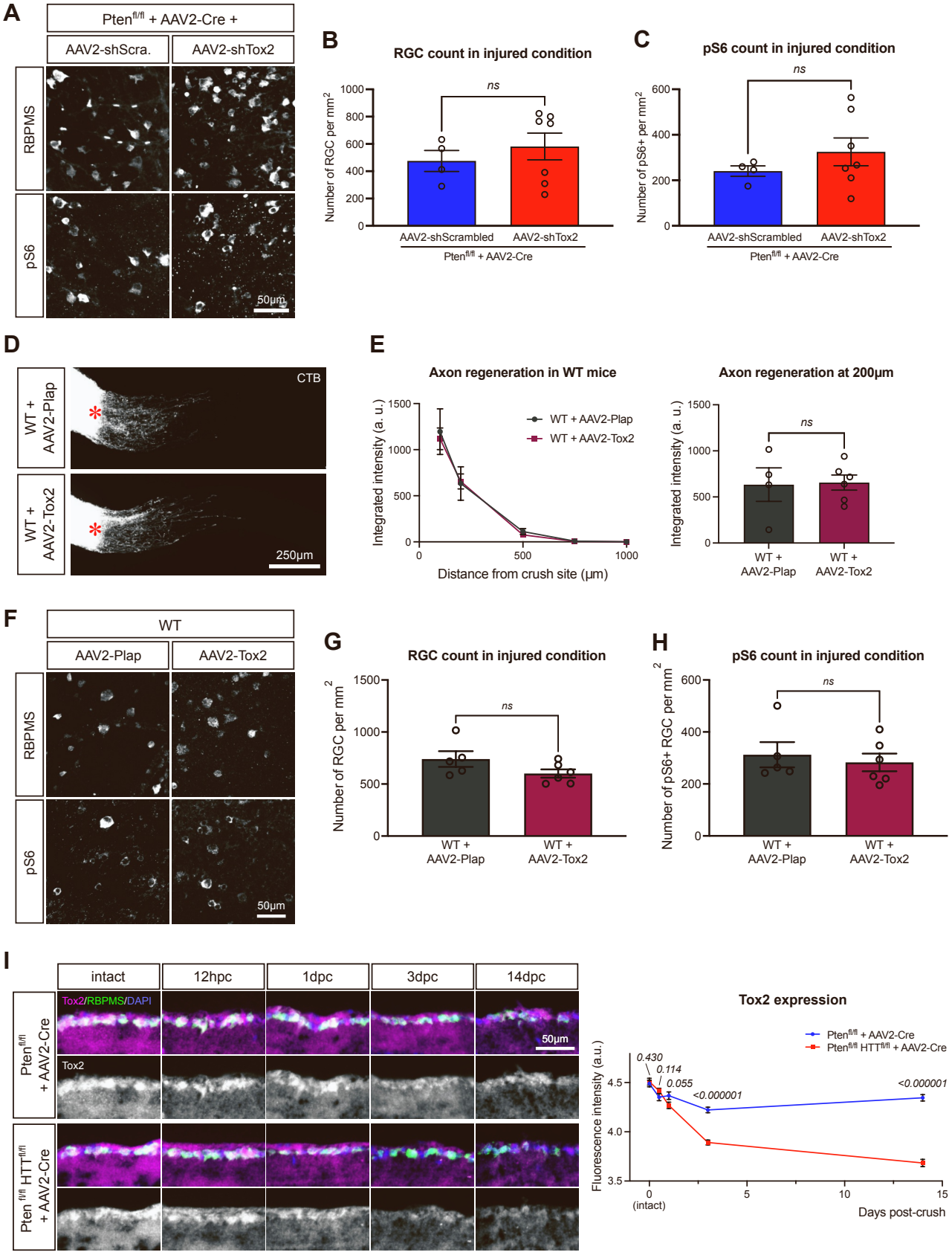

Figure S7: Regulation of Tox2 translation by HTT is necessary but not sufficient to promote axon regeneration in vivo, related to Figure 7.

(A) Whole-mount retina confocal images showing $RBPMS^+$ RGC and $pS6^+$ RGC in $Pten^{fl/fl}$+AAV2-Cre+AAV2-shScrambled and in $Pten^{fl/fl}$+AAV2-Cre+AAV2-shTox2 at 14dpc.

(B) Quantification of $RBPMS^+$ RGC per mm^2 retina at 14dpc. Data are represented as mean +/- s.e.m. Unpaired t-test, ns: not significant.

(C) Quantification of $pS6^+$ RGC per mm^2 retina at 14dpc. Data are represented as mean +/- s.e.m. Unpaired t-test, ns: not significant.

(D) Whole optic nerve confocal images showing CTB^+ regenerating axons WT+AAV2-Plap and WT+AAV2-Tox2 conditions at 14dpc. The injury site is indicated by a red star.

(E) Quantification of integrated fluorescence intensity along the optic nerve. Data are represented as mean +/- s.e.m. Unpaired t-test, ns: not significant.

(F) Whole-mount retina confocal images showing $RBPMS^+$ RGC and $pS6^+$ RGC in WT+AAV2-Plap and in WT^+AAV2-Tox2 at 14dpc.

(G) Quantification of $RBPMS^+$ RGC per mm^2 retina at 14dpc. Data are represented as mean +/- s.e.m. Unpaired t-test, ns: not significant.

(H) Quantification of $pS6^+$ RGC per mm^2 retina at 14dpc. Data are represented as mean +/- s.e.m. Unpaired t-test, ns: not significant.

(I) Representative immunofluorescence images showing Tox2 protein expression in $Pten^{fl/fl}$+AAV2-Cre and $Pten^{fl/fl}HTT^{fl/fl}$+AAV2-Cre retinas, in intact condition and at 12hpc, 1dpc, 3dpc and 14dpc. Quantification of Tox2 immunofluorescence intensity in $Pten^{fl/fl}$+AAV2-Cre and $Pten^{fl/fl}HTT^{fl/fl}$+AAV2-Cre retinas, in intact condition and at 12hpc, 1dpc, 3dpc and 14dpc. Data are represented as mean +/- s.e.m. Multiple t-tests with two-stage step-up method of Benjamini, Krieger and Yekutieli were performed. For each timepoint, the FDR-corrected q-value is displayed.

Supplemental References

[S1] M'Barek, K.B., Pla, P., Orvoen, S., Benstaali, C., Godin, J.D., Gardier, A.M., Saudou, F., David, D.J., Humbert, S., 2013. Huntingtin Mediates Anxiety/Depression-Related Behaviors and Hippocampal Neurogenesis. J. Neurosci. 33, 8608–8620. https://doi.org/10.1523/JNEUROSCI.5110-12.2013

[S2] Shirasaki, D.I., Greiner, E.R., Al-Ramahi, I., Gray, M., Boontheung, P., Geschwind, D.H., Botas, J., Coppola, G., Horvath, S., Loo, J.A., Yang, X.W., 2012. Network Organization of the Huntingtin Proteomic Interactome in Mammalian Brain. Neuron 75, 41–57. https://doi.org/10.1016/j.neuron.2012.05.024